Electronic Supplementary Material (ESI) for RSC Advances.

[*Electronic Supplementary Information (ESI)*]

Directional Mass Transfer of Azo Molecular Glass Microsphere Induced by Polarized Light in Aqueous Immersion Media

Hao Huang,[a] Zenan Wang,[a] Xu Li,[a] Fan Yang,[b] Yechao Su,[c] Jianhong Xu,[c] and Xiaogong Wang*[a]

a. Department of Chemical Engineering, Laboratory of Advanced Materials (MOE), Tsinghua University, Beijing 100084, People's Republic of China.

b. Department of Physics, State Key Laboratory of Low Dimensional Quantum Physics, Tsinghua University, Beijing 100084, People's Republic of China.

c. Department of Chemical Engineering, The State Key Lab of Chemical Engineering, Tsinghua University, Beijing 100084, People's Republic of China.

* Corresponding author. Email: wxg-dce@mail.tsinghua.edu.cn

1. Characterization of the Azo Molecular Glass (IAC-4)

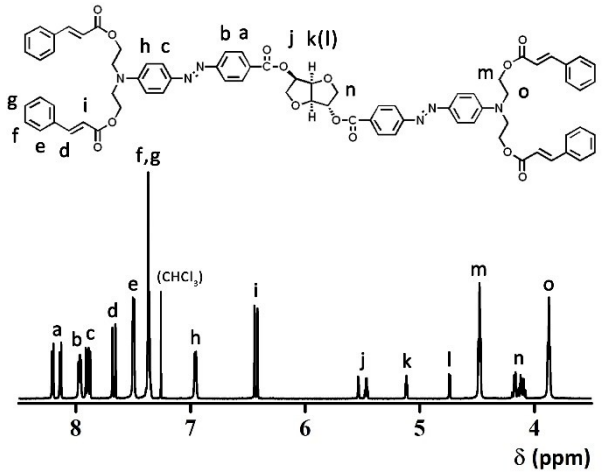

Fig. S1 Chemical structure and ^{1}H NMR spectrum of IAC-4.

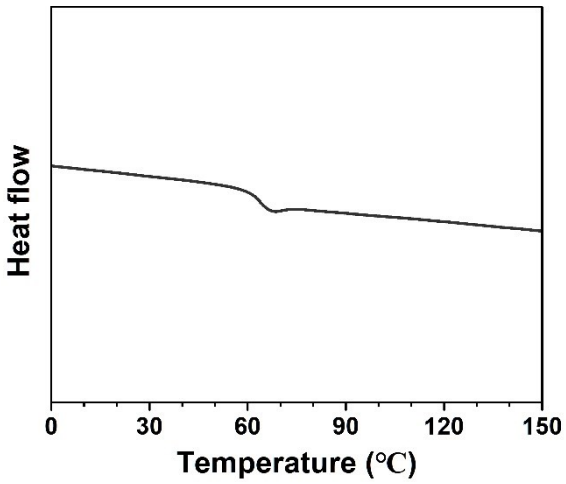

Fig. S2 DSC curve of IAC-4, obtained from the second heating scan. The glass transition temperature (T_g) of IAC-4 was measured to be 64 °C.

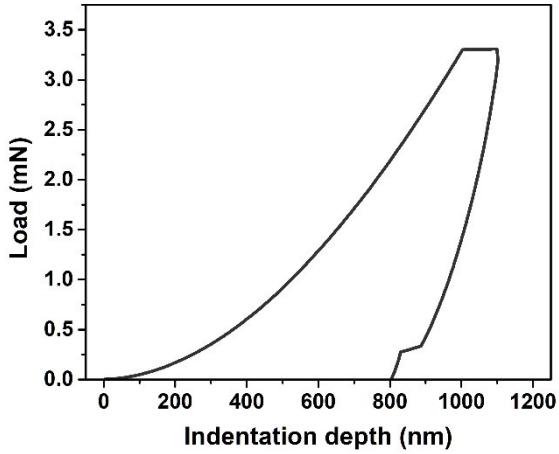

Fig. S3 Nanoindentation curve of IAC-4. The elastic modulus and hardness of IAC-4 were measured to be 3.7 GPa and 0.19 GPa, respectively.

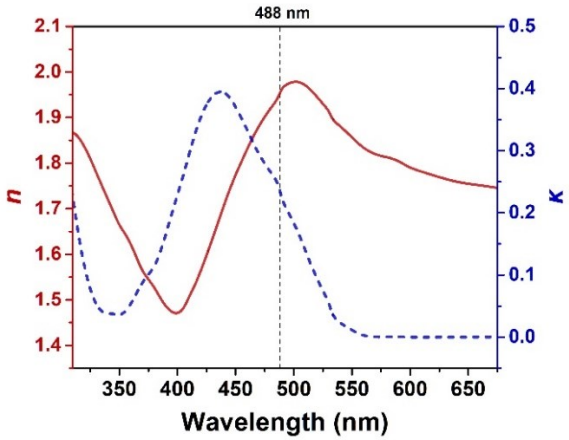

Fig. S4 Spectra of the refractive index (n, red solid line) and extinction coefficient (κ, blue dash line) of IAC-4. The light penetration depth, defined as the propagation distance (z) of light in the material till the transmittance (T) attenuates to 1%, was calculated following the Beer's Law, $T = \exp(-4\pi\kappa z/\lambda_0)$.[S1] At the laser wavelength (λ = 488 nm), n and κ are 1.946 and 0.242, and the light penetration depth is 740 nm.

2. Synthesis and Characterization of Poly(butyl acrylate)

The synthetic procedure of poly(butyl acrylate) (PBA) is as follows. Butyl acrylate (10 g), 2, 2′-azobisisobutyronitrile (AIBN, 0.3 g) and anisole (10 g) were added into a 50 mL Schlenk flask and degassed through three freeze–pump–thaw cycles. The polymerization was carried out in an oil bath at 70 °C for 4 h. After polymerization, the solution was diluted with THF and precipitated in an excessive amount of methanol. The crude product was dissolved in THF and precipitated with methanol again to fully remove the residual monomers. The final product was dried in a vacuum oven at 60 °C for 24 h. T_g: −47 °C. GPC: M_n = 218000, M_w/M_n = 2.38. ^{1}H-NMR (600 MHz, $CDCl_3$, δ (ppm)): 4.01 (m, 2H, O-CH_2-), 2.25 (br, 1H, -CH-), 1.71–1.12 (br, 6H, -CH_2-), 0.92 (t, 3H, -CH_3).

3. Characterization of Immersion Media

Table S1. Physical properties of the immersion media.

	n	Δn [a]	η (mPa·s)	ρ (g/cm^3)
Air [b]	1	-----	1.86×10^{-2}	1.17×10^{-3}
Water	1.333	0.006	0.797	0.996
KSCN solution (30 wt%)	1.394	0.009	1.135	1.162
KSCN solution (52 wt%)	1.448	0.012	1.583	1.301
KSCN solution (70 wt%)	1.491	0.014	3.056	1.413
PVA solution (2.5 wt%)	1.337	0.006	9.316	1.004
PVA solution (5 wt%)	1.340	0.006	89.87	1.010
PVA solution (8 wt%)	1.345	0.006	791.5	1.013

[a]. Mean dispersion (Δn) is defined as the difference of refractive indices at Fraunhofer F-line (λ = 486.1 nm) and C-line (λ = 656.3 nm).

[b]. The viscosity (η) and density (ρ) of air were consulted from the literature (Ref. S2).

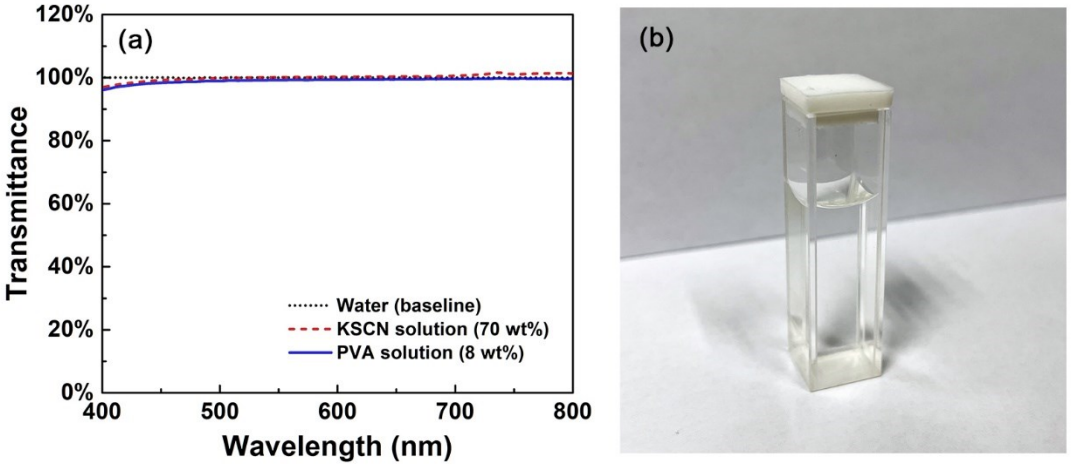

Fig. S5 (a) Transmission spectra of the KSCN solution (70 wt%) and PVA solution (8 wt%), measured in a quartz cuvette with the optical path of 1 cm. The spectrum of deionized water was served as the baseline. As the two solutions both show the high optical transmittance (larger than 99%) at the wavelength of 488 nm, the light attenuation in the immersion media can be neglected. (b) Photograph of the KSCN solution (70 wt%) in the quartz cuvette.

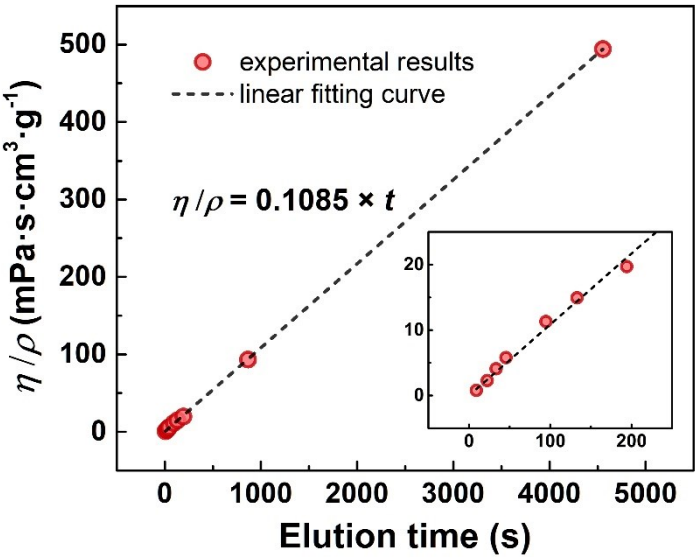

Fig. S6 Calibration curve of Ubbelohde viscometer. The inset is a magnification of the left-bottom region. The calibration was conducted using several standard liquids with the known values of viscosity (η) and density (ρ).[S3,S4] In an ascending order of η, the nine calibration liquids are respectively deionized water, mixtures of isopropanol and diethylene glycol (the mass fraction of diethylene glycol: 0 wt%, 26.1 wt%, 42.9 wt%, 75 wt%, 87.5 wt%, 100 wt%), aqueous solution of glycerin (90 wt%), and glycerin. The result proves that η/ρ is linearly correlated with the elution time (t) in a wide range, which is accordant with the theoretical analysis.[S5] Therefore, the viscosity of the aqueous immersion medium was measured by the Ubbelohde viscometer and calculated using the equation $\eta_{me} = 0.1085 \times t_{me} \times \rho_{me}$.

4. Additional Results of Photoinduced Deformation of IAC-4 Microspheres

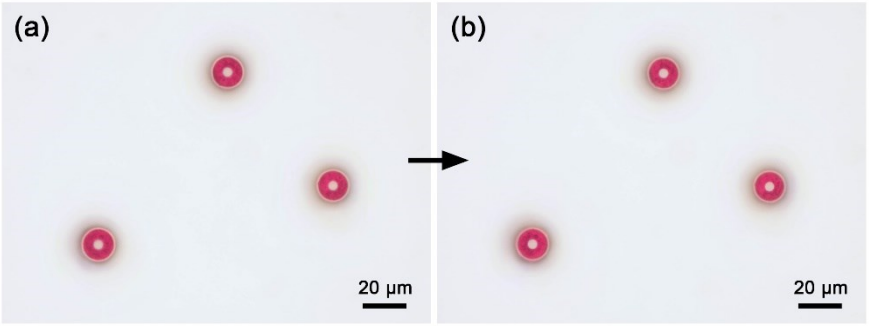

Fig. S7 OM images, (a) the IAC-4 microspheres loaded on the PBA-coated substrate, (b) that after immersed in KSCN solution (70 wt%) for 2 h, washed with plenty of deionized water and dried at ambient condition. The two images were captured in a same region of the same sample. It proves the PBA layer can effectively immobilize the microspheres on the substrate, during the liquid immersion and washing process. In addition, it shows that the concentrated KSCN solution does not corrode or swell the IAC-4 microspheres.

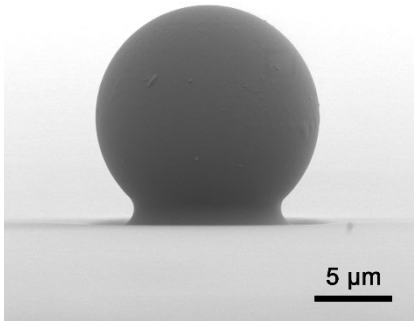

Fig. S8 Front-view SEM image of the IAC-4 microsphere before laser irradiation. The soft PBA layer on the substrate glues the microsphere at the bottom, which exerts enough adhering force, but does not hinder the deformation on the upper part of the microsphere.

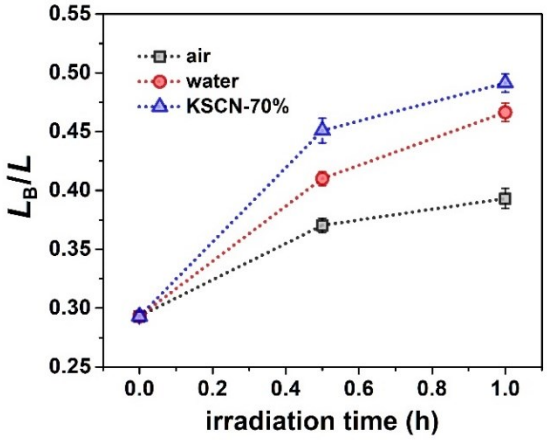

Fig. S9 Variation of L_B/L of the IAC-4 microspheres with the time, irradiated with the linearly polarized light at the wavelength of 488 nm in air, water and KSCN solution (70 wt%).

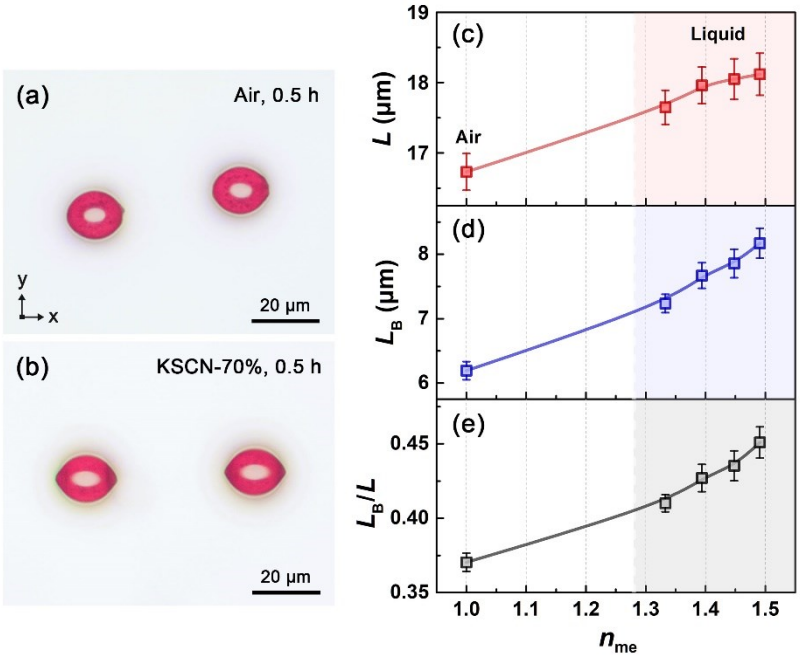

Fig. S10 (a, b) OM images of the photo-deformed particles after irradiated with the linearly polarized light in (a) air and (b) KSCN solution (70 wt%) for 0.5 h. (c) L, (d) L_B and (e) L_B/L of the photo-deformed particles after the irradiation for 0.5 h, plotted versus the refractive index of the immersion medium (n_{me}).

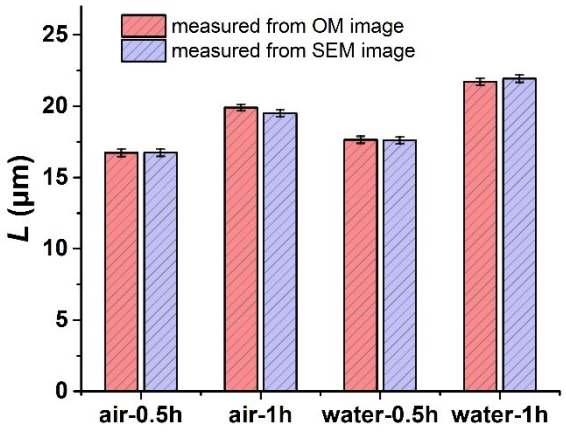

Fig. S11 Comparison of the L values measured from the top-view SEM images and the reflection-mode OM images.

5. Optical Calculation Methods and Results

5.1 Light Refraction and Electric Field at the Interface of Microsphere

Light refraction and electric field at the interface of IAC-4 microsphere with the medium were calculated using Snell's Law and Fresnel Equations.[S6,S7] The model is schematically shown in Fig. S12a. The IAC-4 microsphere with the radius (R) of 7.35 μm is immersed in a

medium and irradiated by the 488 nm linearly polarized light with the intensity of 200 mW/cm^2. The **k** and **E** represent the unit vector of the propagation direction and electric field of the light at the interfaces. A right-handed Cartesian coordinate system is set up with the x-axis parallel to the electric field of the incident light ($\mathbf{E}_0$) and the −z axis along the propagation direction of incident light ($\mathbf{k}_0$). The microsphere center is set as the origin O(0, 0, 0). According to the experimental results, the photoinduced mass transfer mainly occurs parallel to the x- axis and in the z-directions (Fig. 3), which shows no obvious component in the y-axis (Fig. 2g). Consequently, the xOz cross-section of microsphere is selected as the plane of investigation for optical calculation.

In the air, the unit vector of the propagation direction and electric field of the incident light are respectively expressed by,

$$\mathbf{k}_0 = (0,0,-1) \tag{S1}$$

$$\mathbf{E}_0 = E_0(1,0,0) \tag{S2}$$

where E_0 is the electric field amplitude of the incident light.

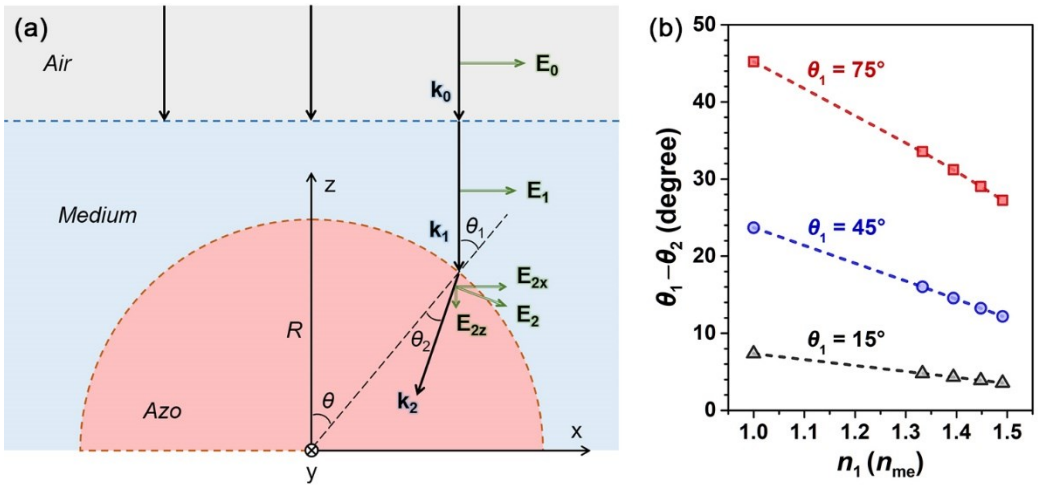

Fig. S12 (a) Schematic illustration of the calculation model. The lower half of microsphere is omitted for clarity. (b) Variation of ($\theta_1 - \theta_2$) with n_1 (i.e., n_{me}), plotted for three different incident angles, 15°, 45° and 75°.

As the light is normally striking the air-medium interface, the light propagation direction vector ($\mathbf{k}_1$) and the electric field ($\mathbf{E}_1$) in the medium shows the same direction with $\mathbf{k}_0$ and $\mathbf{E}_0$, respectively. However, the electric field amplitude in the medium (E_1) is slightly smaller than that in air (E_0) due to the reflection loss at this interface. E_1 can be calculated following the Fresnel equation,[S6]

$$E_1 = \frac{2n_0}{n_0 + n_1} \cdot E_0 = t_{10} E_0 \tag{S3}$$

where n_0 is the refractive index of air, n_1 is the refractive index of the medium (which is termed as n_{me} in the main text), t_{10} (defined as E_1/E_0) is the amplitude transmission coefficient at the air-medium interface.

At the medium-microsphere interface, the point of incidence is represented by (x, 0, z), and the incident angle (θ_1) is always equal with the zenith angle ($\theta = \tan(x/z)$). The refracted angle (θ_2) can be calculated by the Snell's Law,[S6]

$$\theta_2 = \arcsin\left(\frac{n_1}{n_2}\sin(\theta_1)\right) \tag{S4}$$

where n_2 is the real part of refractive index of IAC-4 at the wavelength of 488 nm (which is termed as n_{azo} in the main text). The effect of immersion medium on the light refraction is analyzed using Equation (S4) and illustrated in Fig. S12b.

According to the model (Fig. S12a), in the microsphere, the propagation direction and electric field of the refracted light are respectively expressed by,

$$\mathbf{k}_2 = -\left(\sin(\theta_1-\theta_2), 0, \cos(\theta_1-\theta_2)\right) \tag{S5}$$

$$\mathbf{E}_2 = E_2\left(\cos(\theta_1-\theta_2), 0, -\sin(\theta_1-\theta_2)\right) \tag{S6}$$

As $\mathbf{E}_1$ is parallel to the plane of incidence (xOz plane, see Fig. S12a) without components perpendicular to that, E_2 can be directly calculated by the Fresnel equation,[S6]

$$E_2 = t_{21}E_1 = \frac{2n_1\cos(\theta_1)}{n_2\cos(\theta_1)+n_1\cos(\theta_2)}\cdot E_1 \tag{S7}$$

where t_{21} (defined as E_2/E_1) is the amplitude transmission coefficient at the medium-microsphere interface. Noteworthy, E_2 is the electric field amplitude at the interface (where the propagation distance of refracted light is 0), which can be also termed as the amplitude of transmitted electric field at the microsphere surface.

By combining Equation (S3, S6 and S7), the amplitudes of the transmitted electric field x- and z-components (E_{2x} and E_{2z}) on the microsphere surface can be obtained,

$$E_{2x} = t_{21}E_1\cos(\theta_1-\theta_2) = \frac{2n_1\cos(\theta_1)}{n_2\cos(\theta_1)+n_1\cos(\theta_2)}\cdot\frac{2n_0}{n_0+n_1}\cdot\cos(\theta_1-\theta_2)\cdot E_0 \tag{S8}$$

$$E_{2z} = t_{21}E_1\sin(\theta_1-\theta_2) = \frac{2n_1\cos(\theta_1)}{n_2\cos(\theta_1)+n_1\cos(\theta_2)}\cdot\frac{2n_0}{n_0+n_1}\cdot\sin(\theta_1-\theta_2)\cdot E_0 \tag{S9}$$

The light intensity (I) is proportional to the square of the electric field amplitude,[S6]

$$I = \frac{n}{2c\mu_0}E^2 \tag{S10}$$

where c and μ_0 are respectively the light speed and permeability in vacuum. Consequently, E_2^2 can represent the light intensity (a relative value) of the refracted light at the medium/microsphere interface. The values of E_{2x}^2 and E_{2z}^2 can then be regarded as the intensity of the transmitted electric field x-component and z-component at the microsphere surface, respectively; and there is always $E_2^2 = E_{2x}^2 + E_{2z}^2$. The calculation results are shown in Fig. 8b, 8c and S13.

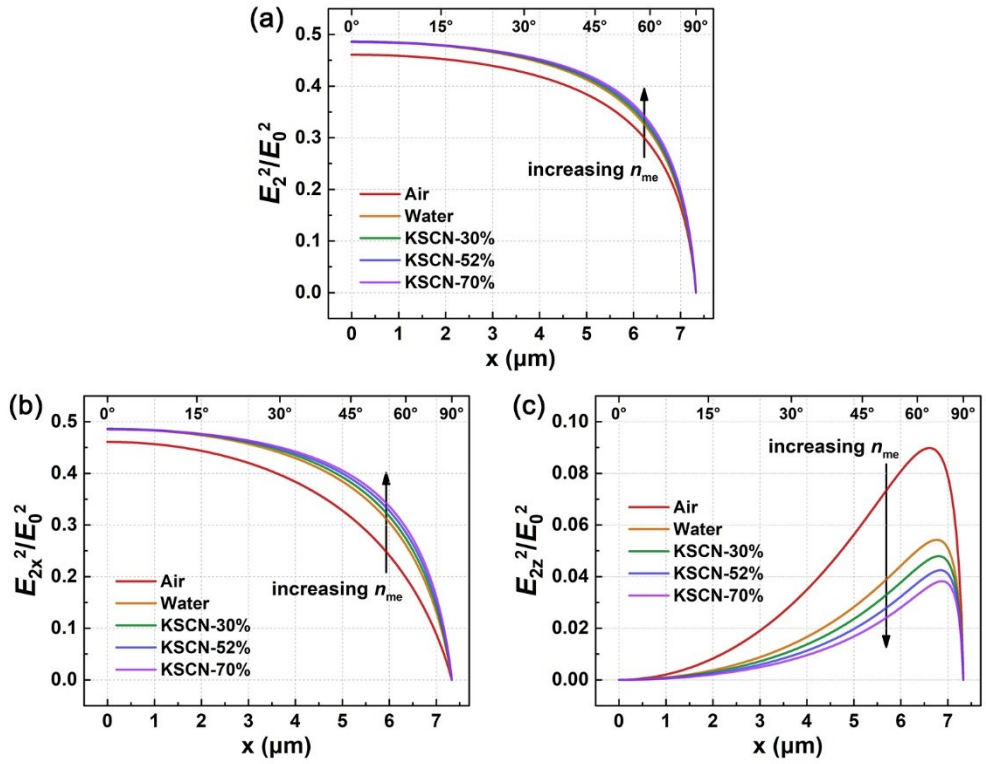

Fig. S13 The square of (a) the total electric field (E_2^2), (b) the x-component (E_{2x}^2), and (c) the z-component (E_{2z}^2) at the upper surface of microsphere relative to the values of the incident light versus the x coordinate for the light irradiation in air, water and the KSCN solutions (30 wt%, 52 wt% and 70 wt%) with different n_{me}. The incident angle is plotted as the top axis.

5.2 Light Refraction and Electric Field at the Interface of Deformed Particles

After the linearly polarized light irradiation, the upper surface profile of the deformed particles is deviated from its original spherical one, which has influences on light refraction and the electric field energy distribution at the interface with the immersion medium. The optical calculation for the photo-deformed particles is described as follows. First, the outlines of the deformed particles in the xOz cross-section were contoured from their front-view SEM images using ImageJ, an open-source image-processing program.[S8] The discrete points (X, Z) of the obtained upper surface profile were fitted by the polynomial $f_n(x)$ of degree n,

$$z = f_n(x) = a_1\left(\frac{x-b}{c}\right)^n + \mathrm{K} + a_i\left(\frac{x-b}{c}\right)^{n+1-i} + \mathrm{K} + a_n\left(\frac{x-b}{c}\right)^1 + a_{n+1} \quad \text{(S11)}$$

where the term $(x\text{-}b)/c$ is used to enhance the numerical effeciency of the algorithm. In practice, choosing n in a range from 4 to 7 can produce a well-fitted smooth curve.

As the incident light propagates along the −z direction, the incident angle (θ_1) at the deformed upper surface can be calculated by,

$$\theta_1 = \left|\text{atan}\left(f_n'(x)\right)\right| \tag{S12}$$

where

$$f_n'(x) = \frac{na_1}{c}\left(\frac{x-b}{c}\right)^{n-1} + \text{K} + \frac{(n+1-i)a_i}{c}\left(\frac{x-b}{c}\right)^{n-i} + \text{K} + \frac{a_n}{c} \tag{S13}$$

For the deformed particles shown in Fig. 3a-d, their contoured outlines and fitted surface profiles are shown Fig. S14, which coincide well with each other. In addition, we also estimated the length of bright spot (L_B) of each surface profile, using the value of L (measured from the corresponding front-view SEM image) and the value of L_B/L (obtained from OM images and averaged), which is labelled in the top axis of Fig. S14. It demonstrates that the incident angle on the edge of bright spot ranges from 16.1° to 17.9°, very close to the theoretical predicted value (16.7°). Hence, the accuracy of the fitting is verified by both the surface profile and the incident angle (the first order derivative of surface profile).

After the incident angle of the deformed surface is obtained using Equation (S11-S13), the electric field is then calculated by Equation (S1-S10) in sequence. The calculation results for the deformed particles are shown in Fig. 8d, e and Fig. S15.

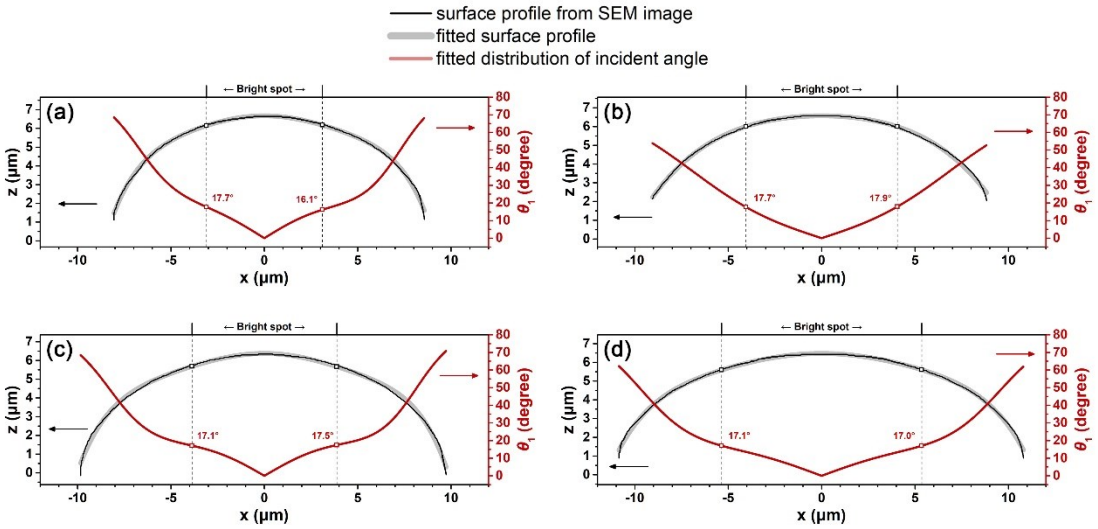

Fig. S14 Polynomial fitting of the upper surface profile in the xOz cross-section of the deformed particles in Fig. 3a-d in the main text. The irradiation with the polarized light is (a, c) in air and (b, d) in KSCN solution (70 wt%), respectively, and the irradiation time is (a, b) 0.5 h and (c, d) 1 h, respectively.

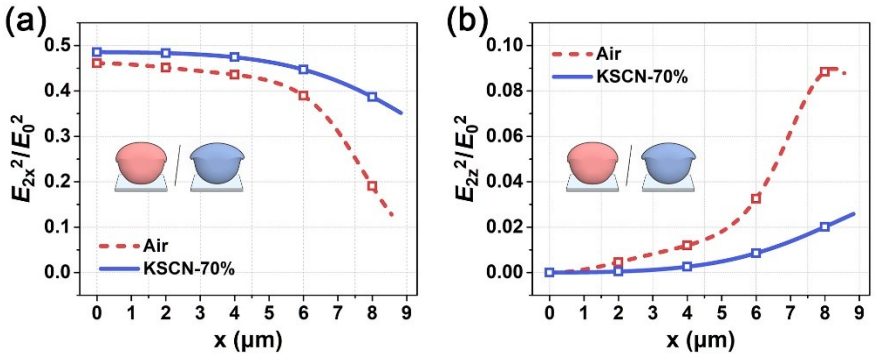

Fig. S15 (a) E_{2x}^2 and (b) E_{2z}^2 at the upper surface of the deformed particles versus the x coordinate after the irradiation with polarized light in air and KSCN solution (70 wt%) for 0.5 h. The values of E_{2x}^2 and E_{2z}^2 were normalized with E_0^2. The calculation uses the cross-sectional profiles given in Fig. S14a, b.

5.3 Light Propagation and Attenuation in IAC-4 Microsphere

In addition, the light propagation and attenuation inside the IAC-4 microsphere were simulated using the ray tracing method.[S9,S10] The detailed calculation procedures are available in Ref. S10, which is not repeatedly described here. As shown by the calculation results (Fig. S16), the light intensity is rapidly attenuated with the propagation distance in the microsphere, which is attributed to the strong optical absorption ability of IAC-4 ($\kappa = 0.242$ at the wavelength of 488 nm, Fig. S4). The employment of the aqueous immersion medium (see Fig. S16b) shows no obvious effect on the light penetration depth. As most of the light energy is absorbed by the surface layer of microsphere, the significant mass transfer induced in this region will dominate the shape deformation process of the microsphere. Consequently, the transmitted electric field intensity (E_2^2, E_{2x}^2 and E_{2z}^2) on the microsphere surface, calculated by the Snell's Law and Fresnel equations, can reasonably explain the distinct photoinduced deformation behavior of IAC-4 microspheres observed for the different immersion media.

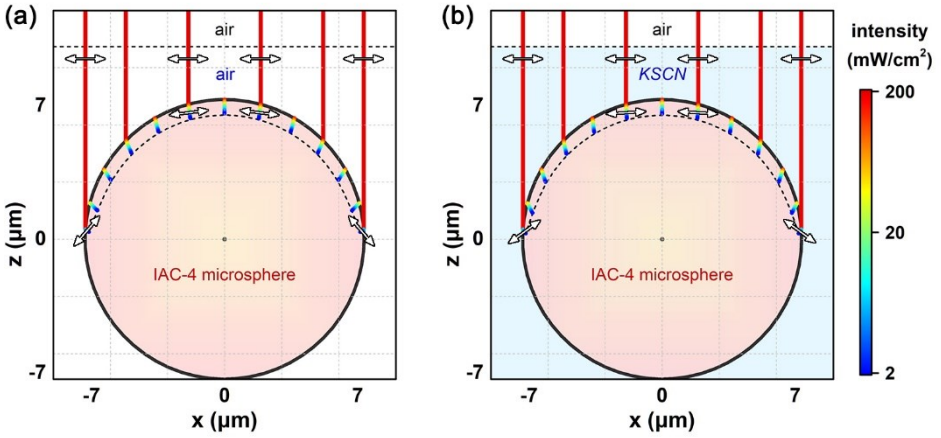

Fig. S16 Propagation and attenuation of 488 nm linearly polarized light in the IAC-4 microsphere, which is immersed in (a) air, (b) KSCN solution (70 wt%). The light propagation is indicated by the colored rays till the points where the intensity is attenuated to 2 mW/cm^2 (transmittance to be 1%). The double-sided arrows represent the electric vibration directions of light in different regions.

6. Fabrication and Photoinduced Deformation of IAC-4 Microarrays

Two types of PDMS molds, which show the periodic hole arrays (PDMS-H, diameter: 500 nm, depth: 700 nm, period: 1 μm) and periodic pillar arrays (PDMS-P, diameter: 950 nm, height: 600 nm, period: 1.4 μm) arranged in the hexagonal lattice on the surface, were purchased from Gdnano Co. Ltd. The micro-pillar arrays and micro-hole arrays of IAC-4 were fabricated from the mold of PDMS-H and PDMS-P, respectively, using a soft-lithographic hot-embossing method reported in the literature.[S11] First, the DMF solution of IAC-4 (5 wt%) was filtered with 0.45 μm syringe membranes and spin-coated onto the clean glass slides with the spinning speed of 1000 rpm. The samples were dried in a vacuum oven at 65 °C for 48 h to remove the residual solvents. The obtained solid films of IAC-4 show the thickness of about 700 nm with smooth surfaces. Then, the PDMS mold containing microstructures was gently pressed on the IAC-4 film, which were kept with seamless touch under moderate pressure (ca. 10 kPa). The samples were heated on a hot-stage at 95 °C and the pressure was maintained for 20 min, during which the PDMS mold was gradually pressed into the molten IAC-4 film under the external force. After the samples were cooled down to room temperature, the PDMS mold was gently peeled off from the surface. The obtained micropatterns on glass substrate show an inverse morphology with respect to the microstructures on PDMS molds. After fabrication, the IAC-4 microarrays were irradiated with the 488 nm linearly polarized light using the experimental setup shown in Fig. 1a in air and the water immersion medium (deionized water). To better control the obtained structures, the light intensity (after the 45° mirror) was set to be 20 mW/cm^2. The morphology of the microarrays before and after the irradiation was characterized by SEM from the top-view, as shown in Fig. S17.

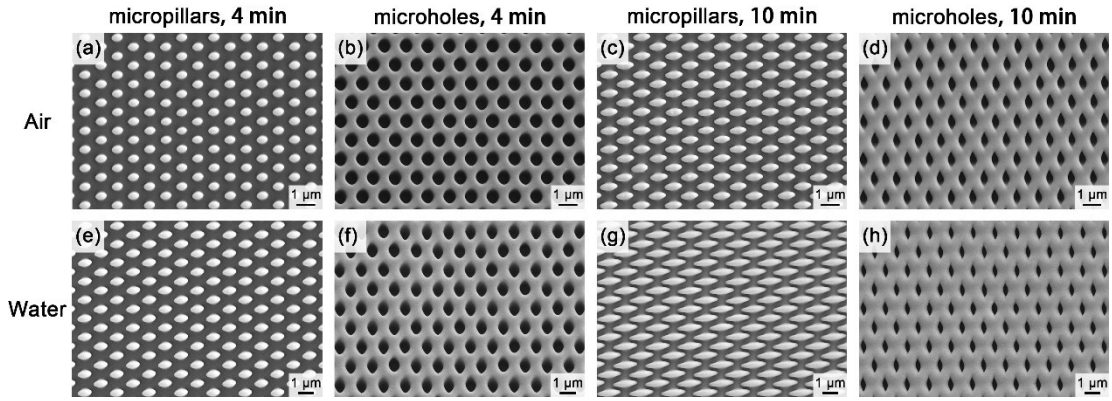

Fig. S17 Top-view SEM images of the IAC-4 microarrays after the 488 nm linearly polarized light irradiation in (a-d) air and (e-h) deionized water for different time periods for the micro-pillar arrays (a, c, e, g) and micro-hole arrays (b, d, f, h) of IAC-4.

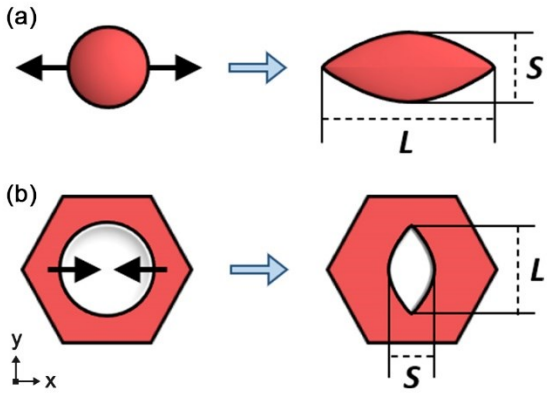

Fig. S18 Schematic illustration of the photoinduced effects, (a) micro-pillar arrays, (b) micro-hole arrays of IAC-4 upon the linearly polarized light irradiation. The definition of *L* and *S* is illustrated in each figure. The coordinate system is indicated in the left-bottom corner of (b).

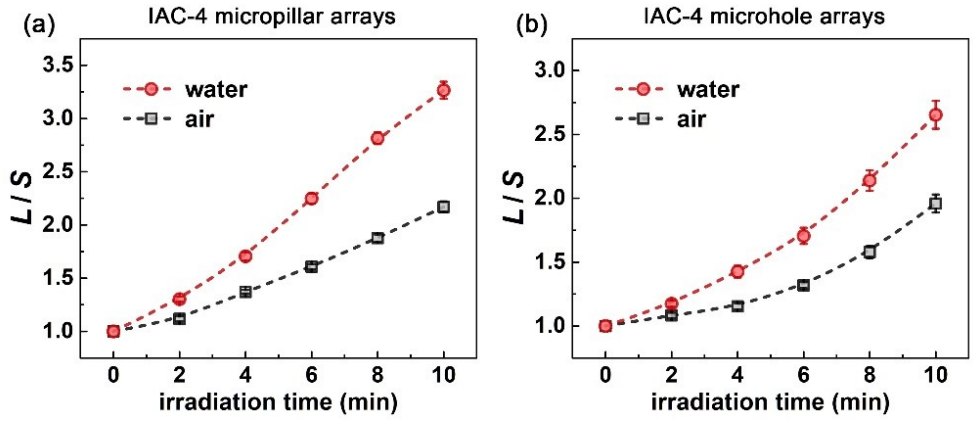

Fig. S19 Variation of the ratio (*L*/*S*), (a) pillar arrays, (b) hole arrays upon the 488 nm linearly polarized light irradiation in air and water for different time periods. Light intensity was fixed to be 20 mW/cm^2 for each case. Some typical SEM images are shown in Fig. S17.

References

[S1] M. Fox, *Optical Properties of Solids*, Oxford University Press, New York, 2001.

[S2] D. Gray, *American Institute of Physics handbook* (3rd ed.), McGraw-Hill, New York, 1972.

[S3] M. L. Sheely, *Ind. Eng. Chem.*, 1932, **24**, 1060-1064.

[S4] M. Almasi, *J. Chem. Eng. Data*, 2012, **57**, 2992-2998.

[S5] S. V. Gupta, *Viscometry for Liquids: Calibration of Viscometers*, Springer International Publishing AG, 2014.

[S6] M. Born and E. Wolf, *Principles of Optics: Electromagnetic Theory of Propagation, Interference and Diffraction of Light* (6th ed.), Oxford, Pergamon, 1980.

[S7] H. Huang, Y. C. Su, X. R. Zhou, C. Y. Liao, C. Hsu, Y. Du, J. H. Xu and X. G. Wang, *Soft Matter*, 2018, **14**, 5847-5855.

[S8] https://imagej.net/ImageJ

[S9] O. N. Stavroudis, *The Optics of Rays, Wavefronts, and Caustics*, Academic Press, New York, 1972.

[S10] H. Huang, C. Zhang, J. X. Lan, Z. N. Wang and X. G. Wang, *Soft Matter*, 2020, **16**, 9746-9757.

[S11] C. Hsu; Z. D. Xu and X. G. Wang, *Adv. Funct. Mater*, 2018, **28**, 1802506.